In-plane polarization anisotropy of ground state optical intensity in InAs/GaAs quantum dots

Muhammad Usman

Citation: Journal of Applied Physics **110**, 094512 (2011); doi: 10.1063/1.3657783
View online: http://dx.doi.org/10.1063/1.3657783
View Table of Contents: http://aip.scitation.org/toc/jap/110/9
Published by the American Institute of Physics

In-plane polarization anisotropy of ground state optical intensity in InAs/GaAs quantum dots

Muhammad Usman[a)]
Tyndall National Institute, Lee Maltings, Dyke Parade, Cork, Ireland

(Received 22 April 2011; accepted 28 September 2011; published online 9 November 2011)

The design of optical devices such as lasers and semiconductor optical amplifiers for telecommunication applications requires polarization insensitive optical emissions in the region of 1500 nm. Recent experimental measurements of the optical properties of stacked quantum dots have demonstrated that this can be achieved via exploitation of inter-dot strain interactions. In particular, the relatively large aspect ratio (AR) of quantum dots in the optically active layers of such stacks provide a two-fold advantage, both by inducing a red shift of the gap wavelength above 1300 nm, and increasing the TM_{001}-mode, thereby decreasing the anisotropy of the polarization response. However, in large aspect ratio quantum dots ($AR > 0.25$), the hole confinement is significantly modified compared with that in lower AR dots—this modified confinement is manifest in the interfacial confinement of holes in the system. Since the contributions to the ground state optical intensity (GSOI) are dominated by lower-lying valence states, we therefore propose that the room temperature GSOI be a cumulative sum of optical transitions from multiple valence states. This then extends previous theoretical studies of flat (low AR) quantum dots, in which contributions arising only from the highest valence state or optical transitions between individual valence states were considered. The interfacial hole distributions also increases in-plane anisotropy in tall (high AR) quantum dots ($TE_{110} \neq TE_{-110}$), an effect that has not been previously observed in flat quantum dots. Thus, a directional degree of polarization (DOP) should be measured (or calculated) to fully characterize the polarization response of quantum dot stacks. Previous theoretical and experimental studies have considered only a single value of DOP: either [110] or [−110]. © *2011 American Institute of Physics*. [doi:10.1063/1.3657783]

I. INTRODUCTION

A. Isotropic polarization response is desirable for optical devices

The electronic structure of single and stacked InAs quantum dots (QDs) has been extensively studied in the last couple of decades for the design of optical devices[1–8] and devices suited to quantum information processing.[9–12] Recent efforts are focused to achieve isotropic polarization response of ground state optical intensity (GSOI) at telecommunication wavelengths (1300–1500 nm).[2,4–7] The polarization response of QD samples is characterized in terms of degree of polarization: $DOP = (TE - TM)/(TE + TM)$, where TE is the traverse electric mode and is measured along an axis in the plane of quantum dot and TM is the transverse magnetic mode measured along the growth [001] axis.[7,13] The design of certain optical devices such as semiconductor optical amplifiers (SOAs) require isotropic polarization response with $DOP \sim 0$. Generally, InAs QDs obtained from the self-assembly growth process[14] have flat shape after the capping process (i.e., aspect ratio AR (height/base) ≤ 0.2).[14–18] In such QDs, the highest few valence band states possess dominant heavy hole character due to the large magnitude of biaxial strain, which splits the heavy hole (HH) and light hole (LH) bands inside the QD region.[1] As a result, the TE-mode becomes much stronger than TM-mode and the $DOP > +0.9$.

Several methods have been explored to reduce the value of DOP. These methods include (1) strain engineering by over-growing the InAs QDs with InGaAs quantum wells, also known as the strain reducing capping layers,[3] (2) inclusion of dilute impurities such as nitrogen "N,"[19] antimony "Sb,"[20] and phosphorous "P,"[21] etc., (3) exploiting the strain interaction between the QDs in multi-layer QD stacks,[2,4,22] and (4) growing large stacks of QDs in the form of columnar QDs.[5,23] Among these techniques, the exploitation of strain interactions between the quantum dot layers in multi-layer QD stacks have shown great potential to generate polarization-insensitive optical transitions at telecommunication wavelengths.[2,4,22,24,53]

B. Aspect ratio of QDs increases above 0.3

Past experimental studies have shown that the size of the QDs increases with the stacking number[12,25,26] in multi-layer QD stacks. Thus, the aspect ratio AR of the QDs in upper layers may increase above 0.3.[2,25] In such QD systems, the first few conduction band and valence band states will be confined in the upper layers (larger QDs). This is because the stronger strain interaction of the larger QDs will push the energy levels of the smaller QDs to higher values.[27,28] As a result, QDs in the upper layers will be optically active; the lower layers of the QDs will not contribute

a)Electronic mail: usman@alumni.purdue.edu.

to the ground state optical emission for reasonably low carrier occupations.[25] Thus, it is of great interest to understand the electronic structure and the polarization properties of the QDs with AR$>$0.3.

C. TE-mode is anisotropic for tall QDs

Past theoretical calculations of polarization dependent optical transitions in single QDs mainly focus on flat QD geometries (AR$=<$0.2).[18,29–31] These studies suggest that the wave function distributions and polarization response of the GSOI are not affected by changes in the height or the diameter of the QD. However, in relatively tall QDs (AR$>=$0.25), typically present in the upper layers of the multi-layer stacks, the confinement and distribution of the hole wave functions considerably changes within the QD region resulting in interfacial confinements. This significantly affects the magnitude of the TE-mode, making it anisotropic in the plane of the QDs, even for QDs with a perfectly circular base. As a result, the conclusion presented in earlier studies, that the polarization response is insensitive to the aspect ratio, no longer remains valid. A quantitative analysis of the polarization response as a function of the QD AR is necessary to fully understand the optical properties of the QDs.

D. Paper sections and summary

This work aims to present a detailed analysis of the GSOI as a function of the QD AR through systematic multi-million atom simulations. The atomistic calculations of strain and electronic structure allows us to incorporate the symmetry-lowering effects caused by QD/GaAs interface roughness and the inequivalence of the [110] and [−110] directions in the underlying zincblende crystal structure.[1,32] Continuum modeling techniques such as the effective mass approximation and k•p approach cannot include these effects and hence fail to incorporate some of the essential physics. A single InAs QD is simulated for this purpose because the separation between the QD layers in the experimental bilayer samples[2,25] is such that there is negligible hybridization of electronic states outside the QDs. Hence, the electronic states are confined in individual QD as atomic states instead of molecular states. The polarization response of such systems can be understood by studying the single QDs.

The paper is organized as follows: Sec. II describes our methodology. The geometry parameters of the simulated system are discussed in Sec. III. Section IV describes our main results and discussions. We first present optical spectra as a function of the QD AR. We demonstrate that the GSOI is dominated by lower valence band states and is more anisotropic for QD AR$>=$0.25. Next, these effects are explained by examining the carrier probability distributions that show interfacial confinements of the valence band states for QDs with AR$>=$0.25.

II. METHODOLOGY

A. Multi-million atom simulator, NEMO 3-D

InAs QDs embedded in a GaAs matrix are simulated using atomistic modeling tool NEMO 3-D.[33–38] NEMO 3-D simulator has previously been applied to study single,[2,27,39,40] bilayer,[2,27,41] and multi-layer stacked[28,35,42,53] QD systems and has demonstrated quantitative agreement with experiments.

B. Strain and piezoelectricity

The atomistic simulations are performed on a large GaAs matrix surrounding the QDs to properly account for the long range impacts of strain and piezoelectric fields. The size of the GaAs box surrounding the InAs quantum dot is chosen large enough to allow strain and piezoelectric fields become zero at the edges of the GaAs box. This ensures proper relaxation of atoms and therefore correctly models the impact of strain and piezoelectric potentials in the calculations of electronic structure. The strain is calculated in atomistic valence force field (VFF) method[43] including anharmonic corrections[38] to the Keating potential. Realistic boundary conditions are chosen for the strain domain:[36] the substrate is fixed at the bottom, the GaAs buffer is periodic in the lateral directions, and the capping layer is free to relax from the top. Linear and quadratic piezoelectric potentials are computed following the procedure described in Refs. 41 and 44.

C. Electronic and optical spectra

The electronic structure calculations are performed by solving empirical tight binding Hamiltonian in which each atomic site is represented by twenty (20) bands in an $sp^3d^5s^*$ model[37] including spin. Electronic domain is chosen to be relatively smaller due to the strong spatial confinement of the electron and hole wave functions inside the QD region. The electronic domain has fixed boundary conditions in all directions. The atoms at the surface are passivated according to our published approach.[36] The inter-band optical transition strengths between the electron-hole energy states are computed using Fermi's golden rule by squared absolute value of the momentum matrix elements summed over spin degenerate states:[41,52] $T_{Ei-Hi} = |< E_i|[\vec{n}, \mathbf{H}]|H_i >|^2$, where $\mathbf{H}$ is the single particle tight binding Hamiltonian in the $sp^3d^5s^*$ basis, E_i is the electron energy state, H_i is the hole energy state, and $\vec{n}$ is the polarization direction. The polarization dependent optical modes are calculated by rotating the polarization vector $\vec{n} = (\vec{x} + \vec{y})\cos\phi \sin\theta + \vec{z}\cos\theta$ to the appropriate direction in the polar coordinates: for the TE_{110}: $\theta = 90°$ and $\phi = 45°$, for the TE_{-110}: $\theta = 90°$ and $\phi = 135°$, and for the TM_{001}: $\theta = 0°$. Here, the angles ϕ and θ are measured from the [100] and [001] axis in the polar coordinate system.

III. SIMULATED QUANTUM DOT GEOMETRY

The schematic diagram of simulated QD system is shown in Figure 1. A lens-shaped InAs QD is embedded inside a GaAs matrix. The QD is placed on the top of a 0.5 nm thick InAs wetting layer. The base diameter, "B," of the quantum dot is kept fixed at 20 nm. The height, "H," of the QD is varied from 2 to 7 nm, corresponding to aspect ratios (AR = H/B) varying from 0.1 to 0.35, respectively. Since the

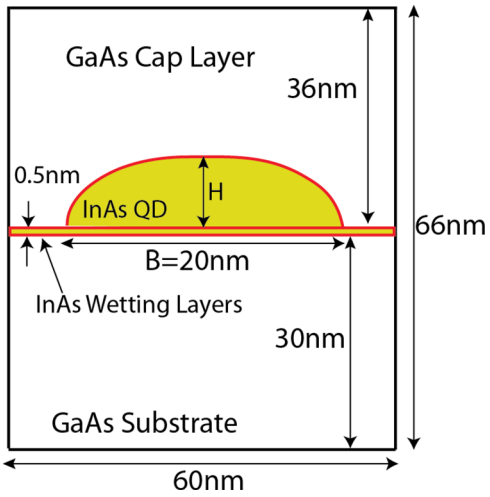

FIG. 1. (Color online) Schematic of simulated quantum dot geometry. A dome shaped InAs quantum dot is embedded inside a GaAs box (matrix). The base diameter, B, of the quantum dot is 20 nm. The height, H, of the quantum dot is varied from 2 to 7 nm, corresponding to a change of 0.1 to 0.35 in the aspect ratio (AR = H/B). The quantum dot is placed on the top of a 1.0 ML thick InAs wetting layer. The size of the GaAs box surrounding the quantum dot is $60 \times 60 \times 66$ nm^3, consisting of ~15 million atoms.

electronic structure of QDs is much more sensitive to changes in their height when compared to the changes in their base diameter,[1,45] we therefore choose to fix the base diameter and increase the aspect ratio by increasing the height of the QD. The size of GaAs buffer for the strain relaxation is $60 \times 60 \times 66$ nm^3 (~15 million atoms) and for the electronic structure calculations is $50 \times 50 \times 56$ nm^3 (~9 million atoms).

IV. RESULTS AND DISCUSSIONS

A. For AR >= 0.25, H3-H5 dominate GSOI

As mentioned earlier in Sec. I, the polarization response of the QD samples is characterized in terms of degree of polarization: DOP = (TE − TM)/(TE + TM). In experimental studies, the TE-mode is measured from a cleaved-edge surface of the QD sample along either the [110] or [−110] direction and the TM-mode is measured along the growth [001] direction.[4,5,7,13,18,46] Figures 2(a)–2(d) show bar plots of normalized TE_{110}-, TE_{-110}-, and TM_{001}-mode optical transition strengths for the QDs with (a) AR = 0.1, (b) AR = 0.2, (c) AR = 0.3, and (d) AR = 0.35. For each AR, we calculate the transition strength $T_{E1\text{-}Hi}$ between the lowest conduction band energy level (E1) and the highest five valence band energy levels (H1-H5). Here, we consider the top five hole energy levels instead of just the top most valence band state H1 because the valence band energies are closely packed and multiple levels can contribute to the GSOI measured at the room temperature.[2]

In Figure 2, for the flat QDs with AR <= 0.2, the optical transition strength from the highest valence band state $T_{E1\text{-}H1}$ is clearly much stronger than the other optical transitions from the lower valence band states: $T_{E1\text{-}H2}$, $T_{E1\text{-}H3}$, $T_{E1\text{-}H4}$, and $T_{E1\text{-}H5}$. Therefore, the GSOI will be dominated by the $T_{E1\text{-}H1}$, and hence, the lower valence band states can be ignored for the calculation of the GSOI. As the QD AR increases to 0.25 and above, the $T_{E1\text{-}H1}$ transition becomes weak, and the lower valence bands exhibit stronger optical strengths. This trend is evident from the Figures 2(c) and 2(d) for the AR = 0.3 and 0.35 cases. We therefore conclude that the experimentally measured GSOI in the tall QDs will be dominated by the emission from the lower lying valence band energy levels as opposed to the flat QDs where the highest valence band state, H1, accounts for almost all of the optical strength.

B. No red shift in optical gap for single QDs when AR is increased

A recent experimental study by E.C. Le Ru *et al.*[22] indicates that increasing the AR (due to increase in the QD height) contributes to a red shift of the emission spectra for bilayer QD samples. However, no such red shift is observed for single QDs with similar change in the AR. They explain that such a difference between single and bilayer QDs could be coming from the bilayer samples where the reduced "In" inter-mixing and the strain interaction between the QDs causes the red shift; these affects are missing in the single QD samples. Our calculations verify the experimental observation about the single QDs that the GSOI peak does not red shift when the QD AR is increased. However, the reason for this difference between the single and bilayer QD spectra also comes from the single QD case: the optical band gap E1-H1 red shifts with increasing AR, but the magnitude of the transition $T_{E1\text{-}H1}$ significantly reduces. For the tall QDs, the $T_{E1\text{-}H1}$ no longer remains dominant, and the main contributions to the GSOI come from the lower lying valence band states, for example, from $T_{E1\text{-}[H3,\ H4,\ H5]}$ in the Figures 2(c) and 2(d).

Figures 2(e)–2(h) plot the transition intensity functions $f(\lambda)_{TE_{110}/TE_{-110}/TM_{001}}$ for QDs with AR = 0.1, 0.2, 0.3, and 0.35, respectively. The same scale on the x-axis is used in all the figures to illustrate the relative position of the GSOI peak as AR increases. In each case, the transition intensity function is computed by placing a Gaussian distribution function with the *mean* at the wavelength of each optical transition, $\lambda_{E1\text{-}Hi}$. The complete mathematical expression is given by Eq. (1). The summation is done over the transition intensities between the lowest conduction band energy level E1 and the highest five valence band energy levels H1, H2, H3, H4, and H5

$$f(\lambda)_{TE_{110}/TE_{-110}/TM_{001}} = \sum_{i=1}^{5} (TE_{110}^{E1-Hi}/TE_{-110}^{E1-Hi}/TE_{001}^{E1-Hi}).e^{\frac{-(\lambda-\lambda_{E1-Hi})^2}{2\sigma^2}}, \text{ where } \sigma = 0.25 \quad (1)$$

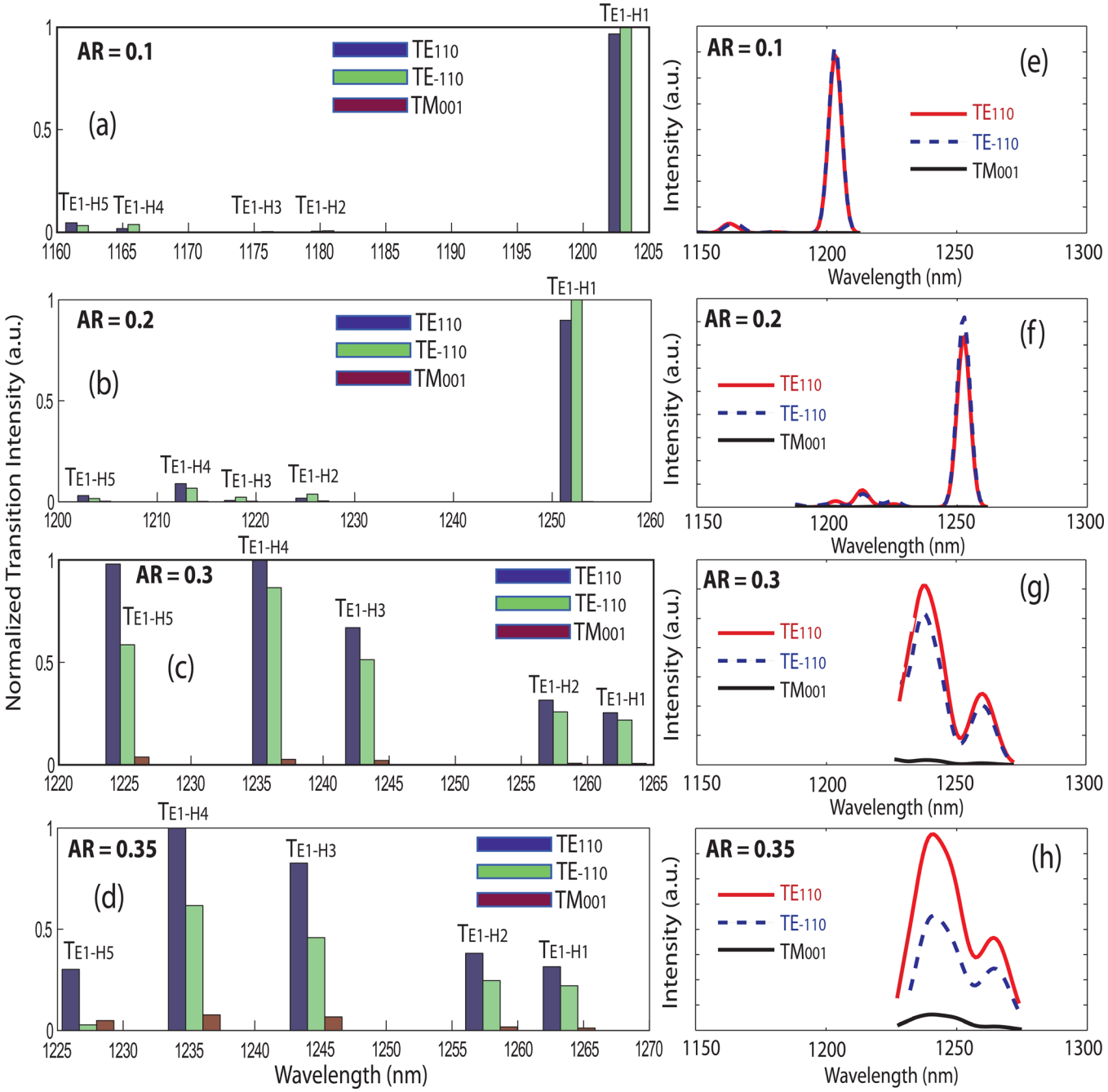

FIG. 2. (Color online) Bar plot of normalized inter-band optical transition strengths between the lowest conduction band state (E1) and the highest five valence band states (H1, H2, H3, H4, and H5) for (a) AR = 0.1, (b) AR = 0.2, (c) AR = 0.3, and (d) AR = 0.35. For each case, the transition strengths are calculated for three polarization directions: TE_{110}, TE_{-110}, and TM_{001}. Different range on the x-axis is chosen in each graph to highlight the wavelengths of the optical transitions. (e)–(h) The plot of transition intensity functions $f(\lambda)$ for TE_{110}, TE_{-110}, and TM_{001} versus the wavelength for the AR = 0.1, 0.2, 0.3, and 0.35. The transition intensity function $f(\lambda)_{TE_{110}/TE_{-110}/TM_{001}}$ in each case is computed by placing a Gaussian function with its *mean* at the location of the optical transition wavelength, $T_{E1\text{-}Hi}$. The summation is done over the lowest conduction band state E1 and the highest five valence band states H1, H2, H3, H4, and H5: $f(\lambda)_{TE_{110}/TE_{-110}/TM_{001}} = \sum_{i=1}^{5} (TE_{110}^{E1-Hi}/TE_{-110}^{E1-Hi}/TE_{001}^{E1-Hi}).e^{\frac{-(\lambda-\lambda_{E1-Hi})^2}{2\sigma^2}}$, where $\sigma = 0.25$. The graphs are plotted with the same scale on the x-axis to compare the shifts of the optical intensity peak.

In the Figures 2(e)–2(h), the comparison of the plots of the transition intensity functions $f(\lambda)_{TE_{110}/TE_{-110}/TM_{001}}$ for the flat (AR = 0.1 and 0.2) and the tall (AR = 0.3 and 0.35) QDs indicates that the GSOI peak red shifts in the flat QDs as the AR increases. A shift of ~50 nm towards higher wavelengths is calculated when the AR increases from 0.1 to 0.2. However, with further increase in the AR, the GSOI peak does not show any further red shift. This is because despite the transition $T_{E1\text{-}H1}$ red shifts to the higher wavelengths; its magnitude is much smaller than other transitions from the lower valence band states. A blue shift of ~15 nm is calculated when the AR increases from 0.2 to 0.3, and only a small red shift (~5 nm) is calculated when the AR further increases from 0.3 to 0.35. Moreover, we compare the peak value of the GSOI plots as a function of the QD AR in Figure 3. A four to five order of magnitude decrease in the optical

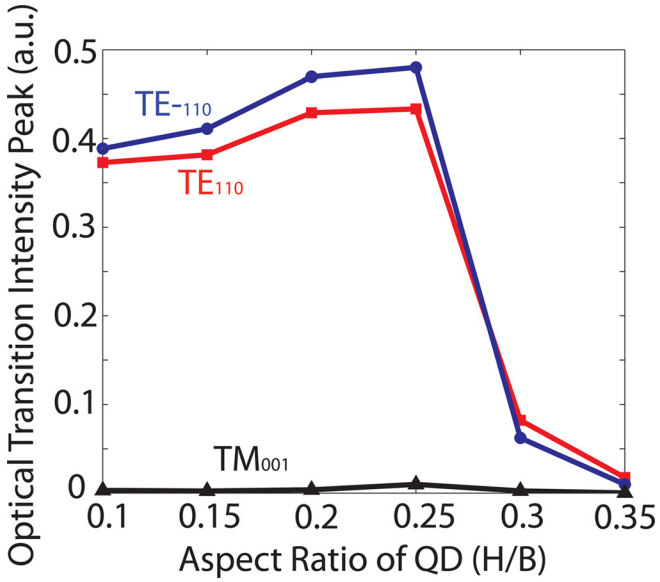

FIG. 3. (Color online) The peak values of the optical intensity plots are plotted as a function of the AR. The optical intensity graphs for the AR = 0.1, 0.2, 0.3, and 0.35 are shown in the Figures 2(e)–2(h). A significant decrease in the optical intensity magnitude is evident for the AR >= 0.3.

intensity is calculated for AR > = 0.3. Later, it will become clear that this is due to the interfacial hole confinements in the tall QDs that actually reduces the electron-hole spatial overlap and hence the transition strength. Therefore, in accordance with experiment,[22] we conclude that the geometry of a single QD cannot be tuned to achieve optical spectra in the wavelength range of interest (1300–1500 nm); the strain interaction between the layers of QDs in the multi-layer QD stacks must be taken into account.

C. Anisotropy of TE-mode

Figure 4 compares the in-plane polarization response of the QDs for the AR = (a) 0.15 and (b) 0.3 cases. The polarization of the incident light is assumed to lie along the [001] direction. The normalized cumulative optical transition intensities between the lowest conduction and the five highest valence band energy states ($T_{E1\text{-}H1} + T_{E1\text{-}H2} + T_{E1\text{-}H3} + T_{E1\text{-}H4} + T_{E1\text{-}H5}$) are plotted in the form of polar plots as a function of the angle ϕ in the plane of the QD. Transverse electric TE-mode strengths along the [110] and [−110] directions (the two commonly measured directions in experiments) are highlighted in Figures 4(a) and 4(b). For comparison, we also show the TE-mode along the [100] and [010] directions, sometimes used to characterize the optical response of the QDs.[47] From the comparison of the two polar plots, it is evident that the TE-mode is anisotropic in the plane of the QDs. Although the difference between the anisotropies of the two polar plots is hard to appreciate from a visual comparison, the two polar plots exhibit significant difference along the two experimentally measured directions: [110] and [−110]. For the QD with AR = 0.15, $TE_{110}/TE_{-110} \sim 0.97$; the polarization response in these two directions is approximately isotropic. However, for the QD with the AR = 0.30, $TE_{110}/TE_{-110} \sim 1.32$ indicating a ~ 32% anisotropy in these two directions. The TE-mode strengths along the other two directions ([100] and [010]) in Figure 4, however, display the opposite trend. The QDs with AR = 0.15 and AR = 0.3 show ~ 22% ($TE_{100}/TE_{010} \sim 1.22$) and ~ 3.4% ($TE_{100}/TE_{010} \sim 1.034$) anisotropies, respectively. The nearly isotropic polarization response along TE_{110} and TE_{-110} for the AR <= 0.2 verifies the results presented in

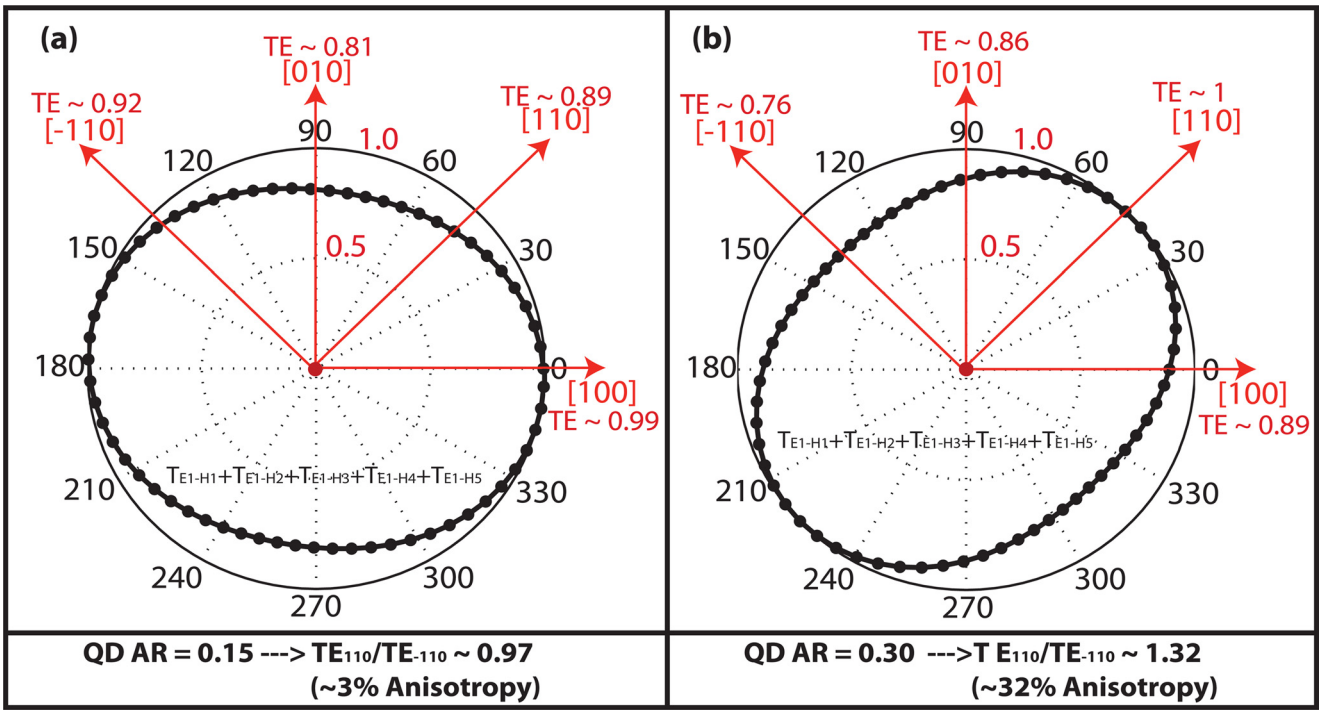

FIG. 4. (Color online) Optical intensity model results represented as polar plots for the QDs with (a) AR = 0.15 and (b) AR = 0.3. The polarization direction of the incident light is kept along the [001] direction. The optical transition strengths are plotted w.r.t the angle ϕ in the plane perpendicular to the growth direction. For both cases, the sum of $T_{E1\text{-}H1}$, $T_{E1\text{-}H2}$, $T_{E1\text{-}H3}$, $T_{E1\text{-}H4}$, and $T_{E1\text{-}H5}$ transition intensities is plotted. The values of the TE-mode along the [100], [010], [110], and [−110] directions are highlighted by using the red color.

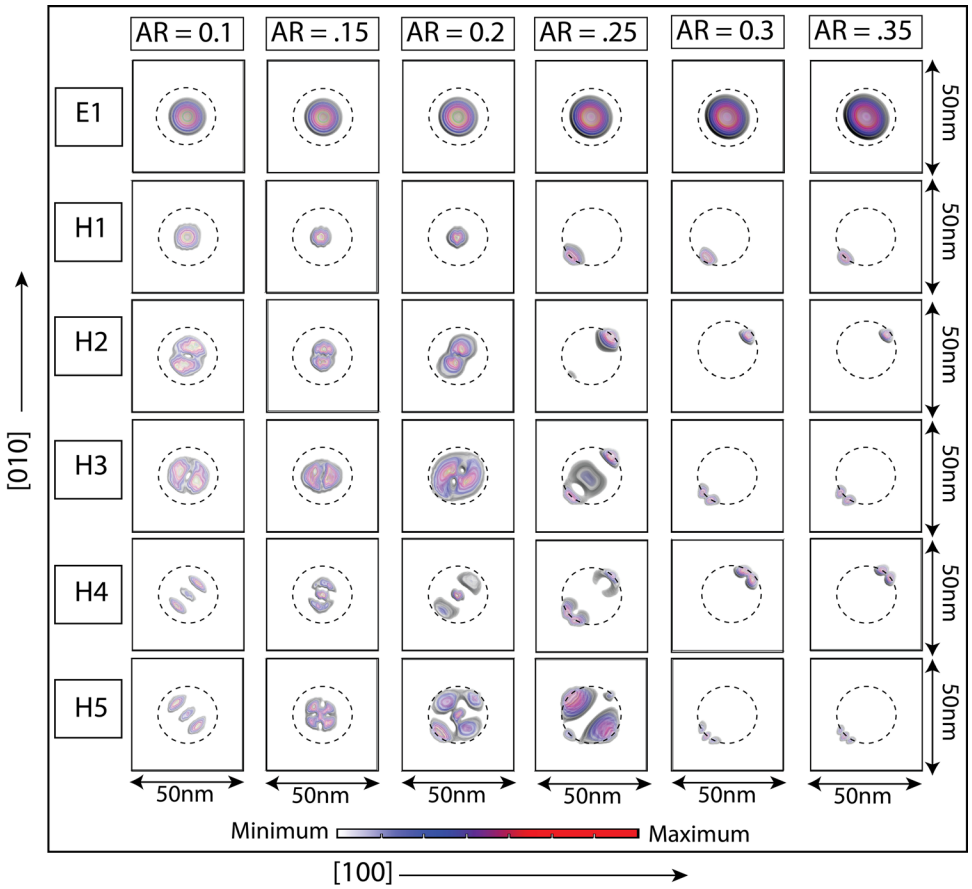

FIG. 5. (Color online) Top-down view of wave function distribution plots for the lowest conduction band state E1 and the five highest valence band states (H1, H2, H3, H4, and H5). The dotted circles mark the boundary of the quantum dots to guide the eye. The square boxes of dimensions 50×50 nm^2 indicate the size of the electronic domain. The intensity of the colors in the plots indicates the magnitude of the wave function: the light blue color representing the minimum value and the red color representing the maximum value.

an earlier theoretical study of flat QDs where an isotropic polarization response was predicted.[30] However, our calculations indicate that the TE-mode strength depends strongly on the geometry of the QD as well as on the direction in the plane of the QD along which it is being measured.

D. Anisotropic "degree of polarization"

We will conclude by highlighting the fact that since the degree of polarization is a function of the TE-mode, it also depends strongly on the chosen direction in the plane of the QD for measurement of the TE-mode. The enhanced anisotropy of the TE-mode in the tall QDs suggests that the DOP is also anisotropic and therefore a single value of the DOP cannot fully characterize the polarization response of such QD samples. Any experimental analysis of the DOP should provide a direction dependent value. Recent experimental and theoretical studies of the PL spectra from the multi-layer QD stacks indicate a highly anisotropic DOP. The authors of Refs. 48 and 53 measure values of -0.36 and $+0.66$ for the DOP along the [110] and [−110] directions, respectively.

E. Interfacial confinements of valence band states

Figure 4 illustrates the anisotropy of the TE-mode optical transitions as a function of the QD AR. In order to understand the source of this anisotropy, we plot spatial distributions of the wave functions for the lowest conduction band energy state E1 and the highest five valence band energy states H1, H2, H3, H4, and H5 in Figure 5. Figure 5 shows the top-down view of the wave function distributions inside the QD region. The dotted circles indicate the boundary of the QD region, and the square boxes (50×50 nm^2) indicate the size of the whole electronic domain. The intensity of the color in the plots represents the magnitude of the wave function: the light blue color indicates the minimum magnitude and the red color indicates the maximum magnitude. The lowest electron wave function E1 demonstrates almost no change as the AR of the QD increases. Only a small spatial spreading of the wave function is observed preserving its overall s-type symmetry.

The hole wave function distributions change significantly as the QD AR increases. For relatively flat QDs (AR $<= 0.2$), the hole wave functions are confined at the center of the QD. As the AR increases to 0.25 and above, the hole wave functions tend to shift towards the interface of the QD along the [110] direction. This change in the orientation and confinement of the hole wave functions explains the nature of the polar plots earlier seen in the Figures 4(a) and 4(b) for the AR $= 0.15$ and 0.3, respectively. For the AR $= 0.3$, the maximum of the polar plot is along the [110] direction because all of the hole wave functions are oriented along this direction. Such spatial orientation of the hole wave functions will cause high polarization anisotropy of the in-plane TE-mode along the [110] and [−110] directions ($\sim 32\%$ for the AR $= 0.3$). In another recent study, Usman *et al.*[2] report $\sim 18\%$ anisotropy of the TE-mode for similar

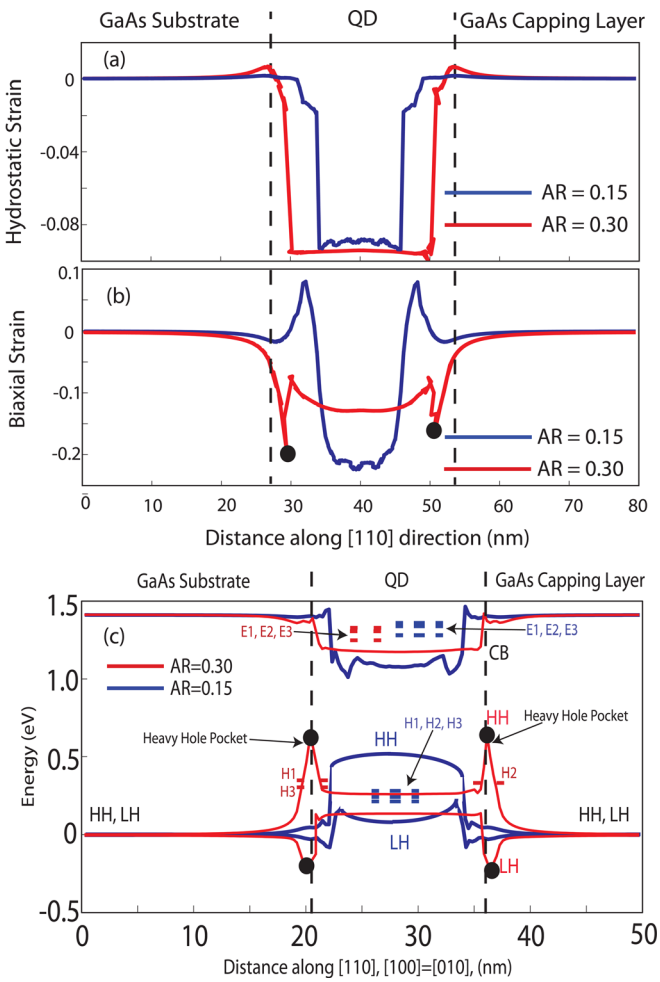

FIG. 6. (Color online) (a) Comparison of the plots of the hydrostatic strain ($\epsilon_H = \epsilon_{xx} + \epsilon_{yy} + \epsilon_{zz}$) in the QDs with the AR = 0.15 and 0.3. The data plotted is obtained along the [110] direction through the center of the QD. (b) Comparison of the plots of the biaxial strain ($\epsilon_B = \epsilon_{xx} + \epsilon_{yy} - 2\epsilon_{zz}$) in the QDs with the AR = 0.15 and 0.3. The data plotted is obtained along the [110] direction through the center of the QD. (c) Comparison of the local band edges in the QD systems with the AR = 0.15 and AR = 0.3. The lowest conduction band (CB) and the two highest valence bands (HH and LH) are shown as a function of the distance along the [110] direction, i.e., [100] = [010]. The positions of the three lowest conduction band energies (E1, E2, and E3) and the three highest valence band energies are specified by using dotted lines.

single QD. The theoretical studies in Refs. 15 and 49 focus on flat QDs and do not indicate any interfacial hole wave function confinements. He *et al.*[50] indicated such interfacial hole confinements for tensile strained InSb/GaSb and compressively strained InAs/GaAs spherical quantum dots due to hole "pockets" in the valence band edges closer to the QD interface where the HH states are trapped. We will show next that similar HH pockets are present in compressively strained InAs/GaAs quantum dots with AR >= 0.25.

F. Biaxial strain creates heavy hole pockets at QD interfaces

The lowest conduction band (CB) is influenced by only hydrostatic strain component ($\epsilon_H = \epsilon_{xx} + \epsilon_{yy} + \epsilon_{zz}$), whereas the heavy hole (HH) and the light hole (LH) valence bands are modified by both the hydrostatic ($\epsilon_H = \epsilon_{xx} + \epsilon_{yy} + \epsilon_{zz}$) and the biaxial strain components ($\epsilon_B = \epsilon_{xx} + \epsilon_{yy} - 2\epsilon_{zz}$).[1] Figures 6(a) and 6(b) compare the hydrostatic and the biaxial strain components, respectively, along the [110] direction. These 1-D cuts are taken through the center of the QD about 1 nm above its base for AR values of 0.15 and 0.3. Here we have chosen the [110] direction because all of the five Hole wave functions are oriented along this direction in the Figure 5 for the AR >= 0.25. The comparison of the hydrostatic strain components indicate that its magnitude only slightly changes at the center of the QD as a function of the AR. A major change however is in its spreading. For the flat QD (AR = 0.15), the hydrostatic strain is very small at the edges of the QD, whereas it has large magnitude in the case of the tall QD (AR = 0.3). This will result in increase in the width of the conduction band energy well and the spreading of the ground state electron wave function. Figure 6(c) plots the lowest conduction band and the highest two valence bands (HH and LH) through the center of QDs along the [110] direction for AR = 0.15 and 0.3. From the comparison of the conduction band edges, it is quite evident that the conduction band well has larger width for the AR = 0.3 when compared to the AR = 0.15. As a result, the lowest conduction band state E1 will be more spread inside the QD region for the AR = 0.3. Figure 5 shows this effect on the spreading of the s-type E1 state.

Figure 6(b) compares the biaxial strain components for QD AR = 0.15 and 0.3. Here we see quite significant difference in the biaxial strain component for the two cases. The biaxial strain component for the flat QD (AR = 0.15) has positive values at the interface of QD and has large negative value at the center of QD. This is typical for flat QDs and has been shown in a number of earlier QD studies.[1,50,51] Such biaxial strain splits the HH and LH bands with opposite order at the center and interfaces of the QD. Figure 6(c) shows that the HH and LH bands for the AR = 0.15 are separated by $\sim$400 meV at the center of the QD. Inside the QD, the HH band is above the LH band and forms an inverted well where the valence band energy states will be confined. The biaxial strain for the AR = 0.3 shows a different profile and has relatively smaller magnitude at the center of the QD. This is because in the tall QDs, the In-As bonds at the center of the QD will feel lesser compressive force from the surrounding GaAs material. More interesting are the negative peaks at the interface of the QD marked by solid black circles. These peaks will create heavy hole and light hole pockets at the interface of QD as can be seen in Figure 6(c), again indicated by the solid black circles. The HH band edge has small wells (pockets) that are higher in the energy than the edge at the center of the QD. The confined states will be trapped inside these pockets and will be concentrated at the interface of the QD. This is quite evident in Figure 5 where the hole states are confined at the QD interface for AR >= 0.25.

V. CONCLUSIONS

The polarization response of InAs quantum dots is studied by using an atomistic modeling technique. Systematic multi-million atom electronic structure calculations are

performed to quantitatively analyze the polarization dependent optical properties of flat (AR <= 0.2) and tall (AR >= 0.25) quantum dots. Such analysis can be applied to understand the polarization response of the multi-layer QD stacks where the size of QDs increases with stacking number and QDs can have AR >= 0.25. Previous theoretical studies only focus on the flat QDs with the AR <= 0.2. The results presented indicate a significant increase in the anisotropy of the TE-mode in the experimentally measured directions ([110] and [−110]) for the tall QDs when compared to the flat QDs. The calculated increase in the anisotropy is due to the interfacial confinements of the valence band states inside the HH pockets created by the biaxial strain. It is therefore proposed that any experimental study of the polarization dependent optical transitions involving tall QDs must consider TE-mode along more than one direction. Moreover, the previous theoretical studies of the ground state optical intensity from the QDs are based on the highest conduction band and the lowest valence band states. This is valid for the flat QDs where this particular transition is dominant and the contributions from the lower valence band states are negligible. However in the case of the tall QDs, the $T_{E1\text{-}H1}$ transition strength becomes weak when compared to the magnitude of the transition from the lower valence band states. Hence, the calculation of the GSOI must be a cumulative sum of the optical strengths from multiple valence band states.

ACKNOWLEDGMENTS

The author gratefully acknowledges Dr. Stefan Schulz and Christopher Broderick of Tyndall National Institute, Lee Maltings, Cork, Ireland, for revising the manuscript and providing valuable suggestions for its improvement. Computational resources provided by Rosen Center for Advanced Computing (RCAC) and http://nanoHUB.org maintained and operated by NSF funded Network for Computational Nanotechnology (NCN) at Purdue University are used in this work. NEMO 3-D simulator is developed by a number of researchers at JPL and Purdue University under supervision of Prof. Gerhard Klimeck (Purdue University) whose work have been cited in the NEMO 3-D references. The open source NEMO 3-D based tools are available at https://nanohub.org/groups/nemo_3d_distribution.

[1]M. Usman, H. Ryu, I. Woo, D. Ebert, and G. Klimeck, IEEE Trans. Nanotechnol. **8**, 330 (2009).
[2]M. Usman, S. Heck, E. Clarke, P. Spencer, H. Ryu, R. Murray, and G. Klimeck, J. Appl. Phys. **109**, 104510 (2011).
[3]J. Tatebayashi, M. Nishioka, and Y. Arakawa, Appl. Phys. Lett. **78**, 3469 (2001).
[4]T. Inoue, M. Asada, N. Yasuoka, O. Kojima, T. Kita, and O. Wada, Appl. Phys. Lett. **96**, 211906 (2010).
[5]P. Ridha, L. Li, M. Mexis, P.M. Smowton, J. Andrzejewski, G. Sek, J. Misiewicz, E. P. O'Reilly, G. Patriarche, and A. Fiore, IEEE J. Quant. Electron. **46**, 197 (2010).
[6]L. Fortunato, M. Todaro, V. Tasco, M. De Giorgi, M. De Vittorio, R. Cingolani, and A. Passaseo, Superlattices Microstruct. **47**, 72 (2010).
[7]P. Jayavel, H. Tanaka, T. Kita, O. Wada, H. Ebe, M. Sugawara, J. Tatebayashi, Y. Arakawa, and T. Akiyama, Appl. Phys. Lett. **84**, 1820 (2004).
[8]P. Ridha, L. Li, A. Fiore, G. Patriarche, M. Mexis, and P. M. Smowton, Appl. Phys. Lett. **91**, 191123 (2007).
[9]M. Bayer, P. Hawrylak, K. Hinzer, S. Fafrad, M. Korkusinski, Z. Wasilewski, O. Stern, and A. Forchel, Science **291**, 451 (2001).
[10]E. Stinaf, M. Schiebner, A. Bracker, I. Ponomarev, V. Korenev, M. Ware, M. Doty, T. Rienecki, and D. Gommon, Science **311**, 636 (2006).
[11]P. Michler, *Single Quantum Dots: Fundamentals, Applications, and New Concepts* (Springer, Berlin, 2003).
[12]H. Krenner, M. Sabathil, E. Clark, A. Kress, D. Schuh, M. Bichler, G. Abstrieter, and J. Finely, Phys. Rev. Lett. **94**, 57402 (2005).
[13]S. C. Heck, S. Osborne, S. B. Healy, E. P. O'Reilly, F. Lalarge, F. Poingt, O. Le Gouezigu, and A. Accard, IEEE J. Quant. Electron. **45**, 1508 (2009).
[14]D. Bimberg *et al.*, *Quantum Dot Heterostructures* (Wiley, New York, 1999).
[15]G. Bester, D. Reuter, L. He, A. Zunger, P. Kailuweit, A. Wieck, U. Zeitler, J. Maan, O. Wibbelhoff, A. Lorke, Phys. Rev. B **76**, 075338 (2007).
[16]D. Bimberg, M. Grundmann, F. Heinrichsdorff, N. Ledentsov, V. Ustinov, A. Zhukov, A. Kovsh, M. Maximov, Y. Shernyakov, B. Volovik, Thin Solid Films, **367**, 235 (2000).
[17]H. Eisele, A. Lenz, R. Heitz, R. Timm, M. Dahne, Y. Temko, T. Suzuki, K. Jacobi, J. Appl. Phys. **104**, 124301 (2008).
[18]W. Sheng and J. P. Leburton, Appl. Phys. Lett. **80**, 2755 (2002).
[19]M. Richter, B. Damilano, J. Y. Duboz, J. Massies, A. Wieck, Appl. Phys. Lett. **88**, 231902 (2006).
[20]H. Liu, M. Steer, T. Badcock, D. Mowbray, M. Skolnick, P. Navaretti, K. Groom, M. Hopkinson, R. Hogg, Appl. Phys. Lett. **86**, 143108 (2005).
[21]J. Jiang, S. Tsao, T. O Sullivan, W. Zhang, H. Lim, T. Sills, K. Mi, M. Razeghi, G. Brown, M. Tidrow, Appl. Phys. Lett. **84**, 2166 (2004).
[22]E. Le Ru, P. Howe, T. Jones, R. Murray, Phys. Rev. B **67**, 165303 (2003).
[23]J. Andrzejewski, G. Sek, E. O'Reilly, A. Fiore, J. Misiewicz, J. Phys.: Conf. Ser. **245**, 012038 (2010).
[24]T. Inoue, M. Asada, O. Kojima, T. Kita, O. Wada, Proc. SPIE **7597**, 75971J-1 (2010).
[25]E. Clarke, P. Howe, M. Taylor, P. Spencer, E. Harbord, R. Murray, S. Kadkhodazadeh, D. McComb, B. Stevens, R. Hogg, J. Appl. Phys. **107**, 113502 (2010).
[26]Q. Xie, A. Madhukar, P. Chen, N. P. Kobayashi, Phys. Rev. Lett. **75**, 2542 (1995).
[27]M. Usman, S. Ahmed, and G. Klimeck, in *Proceedings of 8th IEEE Nano*, Arlington, TX, pp. 541–544 (2008), http://dx.doi.org/10.1109/NANO.2008.161 .
[28]M. Korkusinski and G. Klimeck, J. Phys.: Conf. Ser. **38**, 75 (2006).
[29]A. Williamson and A. Zunger, Phys. Rev. B **61**, 1978 (2000).
[30]A. Williamson, L. Wang, A. Zunger, Phys. Rev. B **62**, 12963 (2000).
[31]A. Williamson, A. Franceschetti, A. Zunger, Europhys. Lett. **53**, 59 (2001).
[32]G. Bester and A. Zunger, Phys. Rev. B **71**, 045318 (2005).
[33]G. Klimeck, F. Oyafuso, T. B. Boykin, R. C. Bowen, P. Von Allmen, Comput. Model. Eng. Sci. **3**(5), 601 (2002).
[34]G. Klimeck, S. S. Ahmed, H. Bae, N. Kharche, S. Clark, B. Haley, S. Lee, M. Naumov, H. Ryu, F. Saied, IEEE Trans. Electron Devices **54**, 2079 (2007).
[35]G. Klimeck, S. S. Ahmed, N. Kharche, M. Korkusinski, M. Usman, M. Prada, T. B. Boykin, IEEE Trans. Electron Devices **54**, 2090 (2007).
[36]S. Lee, J. Kim, L. Jönsson, J. W. Wilkins, G. W. Bryant, G. Klimeck, Phys. Rev. B **66**, 235307 (2002).
[37]T. B. Boykin, G. Klimeck, R. C. Bowen, F. Oyafuso, Phys. Rev. B **66**, 125207 (2004).
[38]O. L. Lazarenkova, P. Von Allmen, F. Oyafuso, S. Lee, G. Klimeck, Appl. Phys. Lett. **85**, 4193 (2004).
[39]S. Ahmed, M. Usman, N. Kharche, A. Schliwa, G. Klimeck, in *Proceedings of IEEE International Conference on Nano/Micro Engineered and Molecular Systems (IEEE-NEMS)*, January 16–19, 2007, Bangkok Thailand, http://dx.doi.org/10.1109/NEMS.2007.352172.
[40]S. Ahmed, M. Usman, C. Heitzinger, R. Rahman, A. Schliwa, G. Klimeck, in *Proceedings of the 28th International Conference on the Physics of Semiconductors, ICPS 2006*, Vienna, Austria, July 24–28, 2006, AIP Conf. Proc. **893**, 849 (2007), http://dx.doi.org/10.1063/1.2730157.
[41]M. Usman, Y. H. Matthias Tan, H. Ryu, S. Ahmed, H. Krenner, T. Boykin, and G. Klimeck, IOP Nanotechnol. **22**, 315709 (2011).
[42]M. Usman, S. Ahmed, M. Korkusinski, C. Heitzinger, G. Klimeck, in *Proceedings of the 28th International Conference on the Physics of Semiconductors, ICPS 2006*, Vienna, Austria, July 24–28, 2006, AIP Conf. Proc. **893**, 847 (2007), http://dx.doi.org/10.1063/1.2730156.
[43]P. Keating, Phys. Rev. **145**, 637 (1966).
[44]A. Schliwa, M. Winkelnkemper, D. Bimberg, Phys. Rev. B **76**, 205324 (2007).

[45]C. Y. Ngo, S. F. Yoon, W. Fan, S. J. Chua, Phys. Rev. B **74**, 245331 (2006).
[46]P. Fry, M. Skolnick, D. Mowbray, I. Itskevich, J. Finley, L. Wilson, K. Schumacher, J. Barker, E. O'Reilly, M. Al-Khafaji, Physica E (Amsterdam) **9**, 106 (2001).
[47]T. Saito, H. Ebe, Y. Arakawa, T. Kakitsuka, M. Sugawara, Phys. Rev. B **77**, 195318 (2008).
[48]Y. Ikeuchi, T. Inoue, M. Asada, Y. Harada, T. Kita, E. Taguchi, and H. Yasuda, Appl. Phys. Exp.**4**, 062001 (2011).
[49]G. A. Narvaez, G. Bester, A. Zunger, J. Appl. Phys **98**, 043708 (2005).
[50]L. He, G. Bester, A. Zunger, Phys. Rev. B **70**, 235316 (2004).
[51]W. Jaskólski, M. Zielinski, G. W. Bryant, J. Aizpurua, Phys. Rev. B **74**, 195339 (2006).
[52]M. Usman, H. Ryu, S. Lee, Y. H. Tan, G. Klimeck, in *Proceedings of 13th International Workshop on Computational Electronics (IWCE)*, Tsinghua University, Beijing, May 27–29, 2009, http://dx.doi.org/10.1109/IWCE.2009.5091140.
[53]M. Usman, T. Inoue, Y. Harda, G. Klimeck, and T. Kita, Phys. Rev. B **84**, 115321 (2011).